REVISION 1

The elasticity of $MgAl_2O_4$-$MnAl_2O_4$ spinels by Brillouin scattering and an empirical approach for bulk modulus prediction

ENRICO BRUSCHINI,[1,*] SERGIO SPEZIALE,[2] GIOVANNI B. ANDREOZZI,[1] FERDINANDO BOSI[1,3] AND ULF HÅLENIUS[3]

[1]Department of Earth Sciences, Sapienza University of Rome, Piazzale Aldo Moro, 5, I-00185 Rome, Italy

[2]Helmholtz Centre Potsdam – GFZ German Research Centre for Geosciences, Potsdam, Germany

[3]Department of Geosciences, Swedish Museum of Natural History, Box 50007, SE-10405 Stockholm, Sweden

ABSTRACT

The elastic constants C_{ij} of a set of synthetic single crystals belonging to the join $MgAl_2O_4$ (spinel sensu stricto) – $MnAl_2O_4$ (galaxite) were determined by Brillouin spectroscopy at ambient conditions. The C_{11} component tends to remain constant for Mg-rich compositions ($X_{Mn} < 0.5$) and decreases in Mn-rich compositions, whereas C_{12} increases and C_{44} decreases almost linearly from $MgAl_2O_4$ to $MnAl_2O_4$. The bulk modulus K_S is weakly dependent upon Mg-Mn substitution within experimental uncertainties, whereas the shear modulus G decreases with increasing Mn^{2+} content. For $MnAl_2O_4$ C_{11} = 271.3(1.3) GPa, C_{12} = 164.8(1.3) GPa, C_{44} = 124.9(5) GPa, Ks = 200(1) GPa and G = 88.7(5) GPa.

Based on the *"polyhedral approach"*, we developed a model that describes the crystal bulk moduli of the $MgAl_2O_4$–$MnAl_2O_4$ spinels in terms of their cation distribution and the polyhedral bulk moduli of the different cations. We refined a set of values for the effective polyhedral bulk modulus of Mg, Mn^{2+} and Al in tetrahedral (T) and octahedral (M) sites, which span from 153 to 270 GPa ranking as follows: $K_{Mn}{}^{M} < K_{Mg}{}^{M} < K_{Mg}{}^{T} \approx K_{Mn}{}^{T} < K_{Al}{}^{M} << K_{Al}{}^{T}$.

* E-mail: enrico.bruschini@uniroma1.it

Crystal bulk modulus was perfectly reproduced within 0.1% for all Mn^{2+}-bearing samples. We also found a high linear correlation between the effective polyhedral bulk modulus and the ionic potential IP of the coordinating cations: $K_i^j(GPa) = 20(2)IP + 108(10)$ (where *i* indicates the cation and *j* the polyhedral site). We tested this simple correlation by calculating the specific effective polyhedral bulk modulus of several cations in T and M coordination and then predicting the crystal bulk modulus for several spinel compositions. The success of our simple correlation in modeling the bulk modulus of spinels outside the $MgAl_2O_4$-$MnAl_2O_4$ system is encouraging, and suggests that the relationships between chemical composition, cation distribution and elastic properties in spinel-structured minerals and materials can indeed be expressed by relatively simple models.

Keywords: Spinels, galaxite, elasticity, Brillouin scattering, cation distribution, crystal chemistry.

INTRODUCTION

A large number of relevant minerals and materials, which are intensively studied in many fields of Earth and Materials Sciences, adopt the spinel structure. Oxide spinels are important accessory minerals in many crustal and mantle rocks and Fe-bearing ringwoodite, the spinel-structured polymorph of $(Mg,Fe)_2SiO_4$, is probably the dominant phase in mantle transition zone (Barnes and Roeder 2001; Frost 2008; Pearson 2014). Materials with spinel structure quite often show remarkable and useful physical properties, such as colossal magnetoresistance, mechanical strength coupled with thermal stability, optical transparency, catalytic activity, etc. (e.g., Grimes 1975; Fabian et al. 2001; Song and Zhang 2004; Fierro et al. 2005; Jörg and Krischanitz 2006; Gelbmann et al. 2013).

Spinel structured compounds have an almost ideal cubic close-packed arrangement of anions (e.g., Hill et al .1979; Sickafus et al. 1999). Considering only one unit cell, the 32 anions produce 64

tetrahedral interstices and 32 octahedral ones. However, only 8 tetrahedral interstices (T) and 16 octahedral interstices (M) are occupied by cations. The general formula of spinel compounds is $^{T}(A_{1-i}B_i)^{M}(A_iB_{2-i})X_4$ where A and B are cations, X are anions and *i* is the inversion degree. In the majority of spinels divalent (A) and trivalent (B) cations can occupy both the tetrahedrally- and the octahedrally-coordinated T and M sites. When all the trivalent cations are in the octahedra (and hence all the divalent cations are in the tetrahedra) the spinel has an inversion equal to zero. The opposite situation occurs when one half of the trivalent cations are in the tetrahedra (and hence all the divalent cations are in the octahedra) and the spinel has an inversion equal to one. Both these configurations can be regarded as ordered. However, most of the natural and synthetic spinels are disordered, with an inversion degree between zero and one. The spinel structure can accommodate a large variety of cations by shifting the anion position along the <111> directions, described by the anion fractional coordinate (*u u u*). Knowing *u* and the unit-cell parameter *a*, it is possible to obtain any geometrical feature (such as bond lengths and bond angles) of the spinel structure.

To date, much effort has been devoted to the experimental and computational study of physical properties of spinel compounds as a function of pressure (Kiefer et al. 1997; Nestola et al. 2002; Levy et al. 2003; Reichmann and Jacobsen 2006), temperature (Askarpour et al. 1993; Andreozzi et al. 2000; Suzuki et al. 2000), and at high magnetic and electric fields (e.g. Hong and Yoo 2006; Ito et al. 2011). Nevertheless, there are still many open issues regarding the dependencies of the physical properties of spinels as a function of composition and crystal-chemistry. In the case of the elastic properties of oxide spinels, most of the literature data is restricted to synthetic end-member compositions or, occasionally, complex natural phases (e.g., Li et al. 1991; Reichmann and Jacobsen 2006 and references therein). The available data are not sufficient to quantify the effect of chemical substitutions on the elastic properties of spinels, even in case of simple binary substitutions. Recently Reichmann et al. (2013) measured the elastic constants of a natural sample with composition $(Mn_{0.40}Fe^{2+}_{0.16}Zn_{0.37}Mg_{0.03})(Fe^{3+}_{1.94}Al_{0.08})O_4$, up to a pressure of ~10 GPa and

compared their results with the end-members franklinite ($ZnFe_2O_4$) and jacobsite ($MnFe_2O_4$) to determine the effect of the Zn-Mn substitution in a natural franklinite. In addition, they also extended their analysis of compositional trends to the large number of spinel-structured compounds (including silicate spinels) for which elastic data are available in the literature and they concluded that there may be deviations from linearity of the single-crystal elastic constants ($C_{ij}s$) and elastic moduli as a function of binary (or more complex) chemical substitutions. However, most of the available literature data are not accompanied by detailed structural and crystal-chemical characterization of the investigated materials and this makes it very difficult to understand in a systematic way how the chemical composition affects the elastic behavior of spinels.

In this study we investigated the single-crystal elastic properties of the solid solution series spinel sensu stricto ($MgAl_2O_4$; Sp) – galaxite ($MnAl_2O_4$; Gx). The full elastic tensors of 4 compositions were determined by Brillouin spectroscopy at ambient pressure and temperature to evaluate the influence of crystal chemistry. To our knowledge, this is the first experimental study of the single-crystal elastic properties of $MnAl_2O_4$ and its solid solution with $MgAl_2O_4$.

MATERIALS AND METHODS

We selected four synthetic, gem-quality single-crystals with different compositions, regularly spaced along the join $(Mg_{1-x}Mn_x)Al_2O_4$, (with x = 0.26, 0.47, 0.76 and 1.00) labeled Gx 50, Gx70, Gx90 and Gx100, respectively. All the samples were synthesized at the very same experimental conditions. The estimated closure temperature was 900 °C. Synthesis details and an in-depth structural, crystal-chemical and spectroscopic characterization of the investigated materials can be found in Hålenius et al. (2007, 2011). According to Hålenius et al. (2007), there are no evidences for the presence of Mn^{3+} in the investigated crystals. This is remarkable, because it is quite uncommon that Fe or Mn are present in only one oxidation state in minerals, even in case of synthetic analogues (e.g., Hålenius et al. 2002; Bosi et al. 2007, 2010; Hålenius and Bosi 2014). In

this study the distinction between total Mn and Mn^{2+} is irrelevant, but in spite of this in the following we will use Mn^{2+} instead of Mn to emphasize that our samples are characterized by the substitution of $Mn^{2+} \rightarrow$ Mg. All the platelets had similar orientation, close to (111), because we ground and polished them starting from well-developed octahedral faces. The platelets were parallel within 0.2-0.3 degree. All the samples were cut, ground and polished in the shape of platelets. The platelets of the different samples had similar orientation being almost parallel to (111), because the starting crystals showed a well-defined octahedral shape. The platelets were then mounted into a sample holder obtained by sandwiching a 250 μm -thick, face parallel, stainless steel disk (with a 2 mm diameter drilled chamber) between two diamond disks. The sample platelets were placed inside the sample chamber in contact with one of the two diamond plates. The main advantage of this assembly for room pressure and temperature Brillouin measurements is the ease of loading and removing the crystals without using any kind of glue or adhesives. In addition, the diamond plate in contact with the sample can act as a very effective heat sink (having a thermal conductivity 10^5 times greater than air) if the sample material partially absorbs the incident laser used for Brillouin scattering measurements.

Brillouin scattering

Brillouin scattering experiments rely on the measurement of frequency shift of light (usually a laser beam) inelastically scattered in the sample (see Speziale et al. 2014 for a review on Brillouin spectroscopy and its application to the Geosciences). When a beam of light is shone on a transparent crystal, a very small fraction of light is inelastically scattered by thermally excited acoustic phonons in the crystal. The acoustic phonons involved in Brillouin light scattering have wavelengths in the 10^2 nm wavelength range. They can be considered as acoustic waves with a linear dispersion relation, and the variation in frequency of light caused by Brillouin scattering is proportional to the acoustic velocity (e.g. Cummins and Shoen 1972). The frequency shift is converted into velocity by knowing the phonon wavevector, which is determined by the

experimental scattering geometry (i.e. the angle between the direction of the incident and scattered beam). In this study, all measurements were performed in forward symmetric (platelet) scattering geometry with an external angle, θ_{ext} of 60°. This scattering geometry allows the determination of the acoustic wave velocity (v) without any knowledge of the sample's refractive index (Whitfield et al. 1976; Sinogeikin and Bass 2000) according to the equation:

$$v = \frac{\Delta\omega\lambda_0}{2\sin\theta_{ext}} \qquad \text{(Eq. 1)}$$

where $\Delta\omega$ is the measured Brillouin frequency shift of the light and λ_0 is the wavelength of the (unshifted) laser light. Brillouin scattering measurements were carried out at the laboratories of the German Research Centre for Geosciences (GFZ) in Potsdam, Germany. The sample assembly described above is then mounted on a 3-circles Eulerian cradle equipped with 3 high-resolution translation stages to allow a precise control of the scattering geometry and the position of the crystal. A six-pass tandem Fabry-Pérot interferometer was used to analyze the scattered radiation (Lindsay et al., 1981). The light source was a Nd:YVO_4 solid state laser operating at a wavelength of 532 nm and polarized at 45° from the vertical direction, that is 45 degrees from the plane containing incident and scattered beams. For each sample 16 to 19 spectra were collected by rotating the crystal along the horizontal axis (which is perpendicular to the platelets facets) in order to probe many different phonon directions within the sample plane. The typical Brillouin spectra of crystalline solids are characterized by two symmetric triplets of peaks corresponding to the 3 polarizations of the acoustic wave propagating in the selected crystal direction. The peaks positions (that is the frequency shifts) were determined by least-square fits to pseudo-Voigt functions and velocities were calculated with equation (1). The full elastic constant tensors and the crystallographic orientations of the sample platelets were refined by performing a non-linear least square fit of the set of Christoffel's equations corresponding to probed acoustic waves (Every 1980). Brillouin scattering of the samples with low amounts of Mn^{2+} (Gx50 and Gx70; see Table 1) was accompanied by luminescence phenomena which took place upon interaction with laser light

(e.g., Tomita et al. 2004). The intensity of luminescence was much stronger at lower Mn^{2+} contents such that it was not possible to carry out measurements of an additional sample with $X_{Mn} = 0.02$.

RESULTS

A representative Brillouin spectrum of the investigated spinel crystals is shown in Figure 1. An example of the measured velocities along with the calculated velocities as a function of rotation angle is shown in Figure 2. The longitudinal wave peak was always observed, and both the shear wave peaks were detected in most of the spectra. In few directions one of the transverse acoustic peaks was absent because of a poor elasto-optic coupling (Cummins and Shoen 1972). The elastic constants of the four Mn-bearing samples are reported in Table 1, together with the estimated uncertainty (1σ), which is always better than 1% of the fitted constanst. For the $MgAl_2O_4$ spinel, we reported in the same table an average of the extant literature data, whose large standard deviation reflects the degree of scattering of the original data. Our results show that, taking into account the standard errors, the elastic tensor component C_{11} has a quite different behavior with respect to C_{12} and C_{44}, which are almost linear as a function of Mn^{2+} content (Fig. 3). In particular, C_{11} remains almost constant from $MgAl_2O_4$ to Gx70, which corresponds to $Mn^{2+} = 0.47$ atoms per formula unit (apfu), and decreases linearly ~4% from the middle of the series to the Mn^{2+} end-member. The value of C_{12} increases almost linearly by 5% as a function of Mn^{2+} content. On the contrary, C_{44} decreases almost linearly (by ~20%). The bulk modulus K_S shows an initial increase from $MgAl_2O_4$ to Gx50 and a decrease from Gx 50 to Gx100. The shear modulus G shows a decreasing trend with Mn^{2+} content (Fig. 4). The observed behavior of K_S is due to the compensation between the trends of C_{11} and C_{12} since $K_S = (C_{11} + 2C_{12})/3$. The trend observed for G is strongly influenced by the C_{44} component as well as by the difference between C_{11} and C_{12}. The elastic anisotropy, expressed by the Zener ratio (Zener 1947) $2C_{44}/(C_{11} - C_{12})$ decreases of 4% from spinel to galaxite.

DISCUSSION

The compositional dependences of C_{12} and C_{44} from spinel to galaxite are anticorrelated. The difference $C_{12} - C_{44}$ increases 17 times across the series from 2.3 GPa to 39.9 GPa. The violation of the Cauchy relationship $C_{12} = C_{44}$ (Born and Huang 1954) indicates the presence of non-central forces acting between the atoms in the structure, Cauchy violation is generally an indication of covalency, due to the fact that central Coulombic forces do not account for it.

A positive violation of the Cauchy relation is observed in all the transition metal oxides with NaCl structure, while the isostructural alkaline earth oxides almost systematically show a negative Cauchy violation. In that case, the positive violation appears to be caused by magnetoelastic effects which weaken C_{44} even at temperatures above the Néel temperature (Jackson et al. 1990 and references within). The spinel structure presents a much different geometric relationship, with larger distances between the tetrahedral Mn atoms, and the magnetic effects should be weaker. In addition, a systematic study of a suite of transition metal cromium spinels (Kocsis et al. 2013) has recently shown that $MnCr_2O_4$ is indeed free of Mn-induced magnetoelastic effects.

A second possible cause of positive Cauchy violation could be the higher covalency of Mn–O bonds with respect to Mg–O at tetrahedral site. However, the optical spectroscopy results by Hålenius et al., 2007, 2011 on the same samples used in this study showed that the crystal field splitting shows a modest decrease along the whole series, and the B Racah parameter, which is inversely proportional to the degree of covalency, fluctuates around a constant value with a slight increase at high Mn contents (Hålenius et al., 2011).

Based on the available information, we think that the compositional dependence of the elastic behavior of the whole series is only marginally due to the increase of covalency associated with Mn/Mg substitution. The dynamical properties of the series are instead controlled by the particular structural flexibility of the spinel structure with respect to substitutions at the tetrahedral site when

the degree of inversion is almost compositional independent such as in the spinel–galaxite series (i.e. Hålenius et al. 2011).

There are few published studies of the systematic dependence of elastic constants of crystals on chemical substitution. Most of them deal with single atomic substitution at the same crystallographic site, as in the series $(Y,Yb)_3Al_5O_{12}$ (Marquardt et al. 2009), KCl-KBr, NaCl-NaBr, and KBr-KI (Giri and Mitra 1986; Slagle and McKinstry 1967). In these cases, all the components of the elastic constant tensor (i.e. C_{11}, C_{12} and C_{44} for cubic crystals) show well-defined linear relations with substituting atom. In more detail, for the series K(Cl,Br), Giri and Mitra (1986) found a perfect linear relation, whereas Slagle and McKinstry (1967) found a slight deviations from the linear trend between the end-members. As a general working hypothesis, we may therefore assume that if the generic ion A^{n+} is replaced by B^{n+} at the same crystallographic site, a linear correlation between elastic constants and chemical composition would be expected, assuming that no structural relaxation occurs around the substituting ion (e.g., Urusov 1992; Juhin et al. 2007; Hålenius et al. 2010, Ardit et al. 2014). However, a more complicated situation can occur as exemplified by the periclase-wüstite series (Mg,Fe)O in which Mg may be replaced by Fe^{2+} or (Fe^{3+} + □), where □ denotes cation vacancies. The latter can be hosted in tetrahedral sites inside the rocksalt structure in compositions with Fe > 0.083 atoms per formula unit (Boiocchi et al 2001). In Fe-rich compositions for charge balance, the accommodation of 2 atoms of Fe^{3+} is always coupled with vacancies according to the formula: $Fe^{2+}_{1-3x}Fe^{3+}_{2x}\square_xO$ with $0.04 < x < 0.12$. A review on wüstite structure and its physical properties is reported by Hazen and Jeanloz (1984). Jacobsen et al. (2002) performed GHz ultrasonic interferometry measurements on a set of crystals belonging to this series and showed that the dependence of the elastic constants from ΣFe/(ΣFe + Mg) can be expressed through second or third order polynomials. In spite of this, the overall behavior of all the elastic constants appears to be not too far from a linear trend. Looking at the crystal-chemical description of these crystals (Jacobsen et al. 2002) it is possible to note that: a) the ratio □/Σcations spans from 0.001 to 0.054; b) the ratio Fe^{3+}/ΣFe spans from 0.01 to 0.13. This implies that the six fold

coordinated Fe^{2+} ($^{VI}Fe^{2+}$) is dominant over $^{VI}Fe^{3+}$, $^{IV}Fe^{3+}$ and cation vacancies. Therefore, in this series, the C_{ij}s variation seems to be mainly driven by the substitution ^{VI}Mg for $^{VI}Fe^{2+}$ which causes an approximately linear trend, while the presence of $^{IV}Fe^{3+}$, $^{VI}Fe^{3+}$ and cation vacancies may cause deviations from linearity.

An early attempts to link the single-crystal elastic properties with the crystal-chemical variations in complex solid solutions was made by Duffy and Vaughan (1988). They measured the elastic constants of a natural Mg-rich orthopyroxene at ambient pressure and temperature and compared their results with those obtained on crystals along the join $MgSiO_3$–$FeSiO_3$. They found a marked non linearity and a non-systematic variation of the $C_{ij}s$ as a function of the substitution $^{VI}Fe \rightarrow {}^{VI}Mg$, which reflects the complex interplay between, crystal–chemistry and elastic properties of natural crystals of different provenance, which have different thermal history and trace-elements contents. In the spinel-type structure, the site population is more complex because cations may disorder over the T and M sites. In addition, cation and anion vacancies can also occur (Sickafus et al. 1999, Fregola et al. 2011). We therefore expect that the compositional dependence of the $C_{ij}s$ in our Mn-bearing spinels is not necessarily linear.

As pointed out by Hålenius et al. (2011), in the $MgAl_2O_4$–$MnAl_2O_4$ series Mn^{2+}, Mg and Al populate both the T and M sites (Table 2). Accordingly, structural variations along the solid solution cannot be exclusively attributed to the substitution $Mn^{2+} \rightarrow Mg$, but also to the distribution of Mn^{2+}, Mg and Al at the T and M sites (where ^{T}Al denotes the inversion degree). In the investigated samples, the inversion degree is characterized by a non-monotonic trend reaching a maximum at the middle of the series (sample Gx 70), and then decreasing toward the $MnAl_2O_4$ end-member (Fig. 5). Due to the observed non-linear behavior of some of the elastic parameters (in particular C_{11} and K_S), it may be hypothesized that elastic properties are a result of different contributions from cations in the various polyhedra that build up the structure.

To understand and possibly quantify the effect of the inversion degree on elastic properties of the investigated crystals, we conducted an analysis based on the so called *polyhedral approach* (e.g.,

Au and Hazen 1985; Hazen 1988). This method has been proven to work satisfactorily under certain conditions, and a model can be constructed relying on the two assumptions discussed in detail by Hazen (1988): *"(1) each type of cation polyhedron has its own characteristic properties (...) which are invariant from structure to structure and (2) bulk crystal properties can be derived from polyhedral properties if appropriate summation procedure are known"*. In a crystal characterized by reduced or no structural degree of freedom (where the polyhedra are not allowed to tilt, rotate or deform anisotropically), the volume variation as a function of pressure will be mainly due to the polyhedral volume variation. If the crystal structure is based on a single type of polyhedron (e.g., octahedra in NaCl structure), the bulk modulus of the entire crystal has to be equal to the bulk modulus of the polyhedron. Otherwise, if the crystal is made up of two or more polyhedra with different bulk moduli, each polyhedron will contribute to the crystal bulk modulus proportionally to its abundance in the structure. The latter case applies to spinels, that are also characterized by solid solution over the non-equivalent sites. In building our model we started from the observation by Finger et al. (1986) that for spinels the crystal bulk modulus K is approximately equal to the average of the polyhedral bulk moduli. According to Finger et al. (1986), if K^T is the tetrahedral bulk modulus and K^M is the octahedral bulk modulus then the crystal bulk modulus tends to be equal to $(K^T + K^M)/2$. However, considering that in a spinel we have two octahedra for each tetrahedron it seems to be more appropriate to assume that the crystal bulk modulus corresponds to:

$$K^{crystal} = \frac{K^T + 2K^M}{3} \qquad \text{(Eq. 2)}$$

Generalizing the problem to a crystal containing *m* cations disordered over *n* different polyhedra, we can describe the bulk modulus by:

$$K^{crystal} = \sum_{i=1}^{m} \sum_{j=1}^{n} \frac{K_i^j X_i^j}{C} \qquad \text{(Eq. 3)}$$

where K_i^j is the bulk modulus of the *i*-th cation in the *j*-th polyhedron, X_i^j is its abundance expressed as atoms per formula units and *C* is the total number of cations per formula unit. Applying this model to the $MgAl_2O_4$–$MnAl_2O_4$ series we can therefore write:

$$K^{crystal} = \left(K_{Al}^T X_{Al}^T + K_{Mg}^T X_{Mg}^T + K_{Mn}^T X_{Mn}^T + K_{Al}^M X_{Al}^M + K_{Mg}^M X_{Mg}^M + K_{Mn}^M X_{Mn}^M\right)/3 \quad \text{(Eq. 4)}$$

According to Eq. 4 the polyhedral bulk moduli (K^T for the tetrahedron and K^M for the octahedron) can be calculated as the linear combination of each specific bulk modulus of the constituent cation in a given polyhedron multiplied by its site abundance over the number of cations (per formula unit) in the polyhedron.

To implement the model, we needed a set of values for the specific bulk moduli of the constituent cations in the polyhedra, namely: K_{Al}^T, K_{Mg}^T, K_{Mn}^T, K_{Al}^M, K_{Mg}^M, K_{Mn}^M. The values for K_{Mg}^M and K_{Mn}^M were taken from simple oxides having NaCl structures (Webb et al. 1988; Speziale et al. 2001 respectively) in agreement with the assumption (1) of Hazen (1988). The other four variables (K_{Al}^T, K_{Mg}^T, K_{Mn}^T, K_{Al}^M) were optimized by minimizing the residuals between calculated and observed crystal bulk modulus of present Mn-spinels through a least-squares fitting of Eq. 4. The bulk modulus of $MgAl_2O_4$ was not used for the minimization routine because, as previously mentioned, it is an average value derived from unknown cation distributions.

The obtained results were excellent as the differences between observed and calculated K values are below 0.1% for all Mn-bearing samples. With respect to $MgAl_2O_4$ composition, the K value calculated from the model is about 1% higher than the average value of literature data and falls within the 1σ standard deviation of such an average. The polyhedral bulk moduli K^T and K^M obtained from the model exhibit non-monotonic opposite trends as a function of the Mn^{2+} total content (Fig. 6). In particular, K^T shows the largest variation, with a maximum difference of ~10 GPa between the samples Gx70 and Gx100, whereas K^M shows an inverse but less pronounced curvature, with a maximum difference of ~2 GPa between the same samples. It is noteworthy that

the trend observed for K^T is parallel to that of the inversion degree, as in both cases the highest value is recorded for sample Gx70 and the lowest for Gx100. This is reflected in the high linear correlation ($R^2 = 0.99$) observed between polyhedral bulk moduli and inversion degree (Fig. 7).

The refined specific polyhedral bulk moduli are largely different from each other and can be ordered as follows: $K_{Mn}{}^M < K_{Mg}{}^M < K_{Mg}{}^T \approx K_{Mn}{}^T < K_{Al}{}^M << K_{Al}{}^T$ spanning from 153 to 270 GPa (Table 3). The trend observed in Fig. 6 and the relationships highlighted in Fig. 7 can be explained considering the extremely different values of the specific tetrahedral bulk moduli $K_{Al}{}^T$ (~270 GPa) compared to $K_{Mg}{}^T$ and $K_{Mn}{}^T$ (both around 180 GPa) as well as the largely different values of ^{T}Al along the series (Table 2). The large variation of K^T along the series is counterbalanced by K^M which has two times higher influence on the crystal bulk modulus (Eq. 2) and this explains the apparent invariance of this latter along the series (Fig. 6).

Notably, the sample Gx100 has the lowest content of Al at the T-site (Table 2) which leads to the lowest value of K^T in the series, only partly counterbalanced by the high content of Al in M-site which gives the highest K^M along the series (Fig. 6).

Our data demonstrates that the tetrahedral bulk modulus is always higher than the octahedral one for any investigated cation (i.e. Mg, Mn^{2+}, Al). This is reasonable considering that the bulk modulus is proportional to the average bond strength which in turn reflects the ionic potential (*IP*, e.g. Bosi et al. 2011), that is formal valence z over ionic radius r, of the various cations (e.g., Velbel 1999). The latter relationship is illustrated by the linear correlation between the refined values of specific polyhedral bulk moduli (K_i^j, expressed in GPa) and the ionic potential (*IP*, expressed as unit valence over ångström) of the various cations (Fig. 8):

$$K_i^j = 20(2)IP + 108(10) \qquad \text{(Eq. 5)}$$

It is worth noting that the observed relationship further supports the empirical relation found by Hazen (1988) in which the polyhedral volume compressibility (that is the inverse of the polyhedral

bulk modulus) is proportional to the cation−anion bond distance and to the formal valence of the cation coordinating the polyhedra.

The approach that we propose allows the prediction of the crystal bulk modulus of a spinel starting from its cation distribution and from the knowledge of the specific polyhedral bulk moduli of its constituent cations. In particular we refined a set of specific polyhedral bulk moduli for Mg, Mn^{2+} and Al (Table 3) and we also observed a close correlation between the fitted values of the specific polyhedral bulk moduli and the ionic potential, *IP*, of the cations (Fig. 8 and Eq. 5). Therefore combining our model (Eq. 3) with Eq. 5 it is possible to predict the bulk modulus of a spinel provided that its cation distribution is known.

IMPLICATIONS

Minerals and materials with spinel structure have a great relevance in Geosciences and for technological applications, respectively. The possibility to predict their bulk modulus starting from chemical composition would have high impact, because may help understanding physical properties of Earth interior as well as designing new materials with tunable elastic behavior. Accordingly, to test the strategy developed in this work, the bulk modulus of several spinel compound was calculated and compared with the experimental data. The first case study was gahnite ($ZnAl_2O_4$): in this spinel Zn is known to be almost completely ordered at the T site while Al is ordered at the M site (Lucchesi et al. 1998; O'Neill and Dollase 1994; Andreozzi et al. 2001, Bosi et al. 2011) and, using an ionic radius of 0.57 Å for the tetrahedrally-coordinated Zn (Bosi et al. 2011), we estimated a value of 179 GPa for K_{Zn}^{T}. The resulting crystal bulk modulus for $ZnAl_2O_4$ calculated according to our model is 198 GPa which, neglecting the difference between K_T and K_S (which is usually in the order of 1-2% for the most common oxide and silicate minerals), is in excellent agreement with the experimental isothermal bulk modulus of 201.7 GPa measured by Levy et al. (2001). We tentatively extended the present model to franklinite ($ZnFe_2O_4$) for which both values of the specific

polyhedral bulk moduli have to be estimated from Eq. 5. As stated before Zn^{2+} has a strong T site preference and this restrains Fe^{3+} to be ordered at the M sites (O'Neill 1992; Waerenborgh et al. 1994; Lucchesi et al. 1999). We used the $K_{Zn}{}^{T}$ previously obtained and estimated $K_{Fe3+}{}^{M}$, then we calculated a crystal bulk modulus of 165 GPa. Also in this case the obtained result is in excellent agreement with the experimental value of 166 GPa (Levy et al. 2000). Very good agreement were also obtained with other oxide spinel compositions having ordered cation distributions, such as Co_3O_4, $FeCr_2O_4$ and $ZnCr_2O_4$. Crystal bulk modulus was reproduced within 3% for the Co-spinel (205 GPa against an experimental value of 199 GPa by Bai et al. 2012), while for the Cr-spinels ($FeCr_2O_4$ and $ZnCr_2O_4$) the calculated crystal bulk moduli (195 and 196 GPa respectively) agree within 7% with the experimental values of Nestola et al. (2014) and Levy et al. (2005; 184.8 and 183 respectively). Our empirical approach does not properly fit the bulk moduli of silicate spinels, which are of great relevance in the Geosciences, in fact when we applied our strategy to the case of spinel-structured $(Mg,Fe)_2SiO_4$ a significant disagreement was observed (about 30% with respect to Hazen 1993). This is probably due to the large difference between the incompressibility of Si-centered tetrahedra with respect to alkaline-earth or transition metal centered ones.

On one hand, such a disagreement suggests that the present strategy needs to be further developed to incorporate a larger base of data to better refine the relationship between ionic radius, nominal valence and polyhedral modulus. On the other hand, however, considering that Eq.5 is only based on the fitted K_i^j values of four samples along the series $MgAl_2O_4$-$MnAl_2O_4$, it is notable that our approach was successful even outside the series used to infer the correlation. We are confident that, when more experimental data linking elasticity and crystal chemistry will be available, it will be possible to express in a relatively simple form the relationship between crystal-chemistry and bulk modulus of a wider range of spinels of general composition. The relevance of such a predictive capacity is very high keeping in mind the dual nature of spinels, able to help understanding physical properties of Earth interior as well as designing new materials with tunable elastic behavior.

ACKNOWLEDGMENTS

Funding by Sapienza University of Rome (Prog. Università 2009, 2011 to Andreozzi G.B.) is gratefully acknowledged. A first version of the manuscript benefited from constructive suggestions of two anonymous reviewers and handling of AE Kristina Lilova.

REFERENCES

Andreozzi, G.B., Lucchesi, S., Skogby, H., and Della Giusta, A. (2001) Composition dependence of cation distribution in some synthetic $(Mg,Zn)(Al,Fe^{3+})_2O_4$ spinels. European Journal of Mineralogy, 13, 391-402.

Andreozzi, G.B., Princivalle, F., Skogby, H., and Della Giusta, A. (2000) Cation ordering and structural variations with temperature in $MgAl_2O_4$ spinel: An X-ray single-crystal study. American Mineralogist, 85, 1164-1171. Erratum, 86, 204.

Ardit, M., Dondi, M., and Cruciani, G. (2014) On the structural relaxation around Cr^{3+} along binary solid solutions. European Journal of Mineralogy, DOI 10.1127/0935-1221/2014/0026-2375.

Askarpour, V., Manghnami, M.H., Fassbender, S., and Yoneda, A. (1993) Elasticity of single-crystal $MgAl_2O_4$ spinel up to 1273 K by Brillouin spectroscopy, Physics and Chemistry of Minerals, 19 (8), 511-519.

Au, A.Y., and Hazen, R.M. (1985) Polyhedral modeling of the elastic properties of corundum (a-Al_2O_3) and chrysoberyl (Al_2BeO_4). Geophysical Research Letters, 12, 725-728.

Bai, L., Pravica, M., Zhao, Y., Park, C., Meng, Y., Sinogeikin S.V., and, Shen, G. (2012) Charge transfer in spinel Co_3O_4 at high pressures. Journal of Physics: Condensed Matter, 24, 435401.

Barnes, S.J., and Roeder, P.L. (2001) The range of spinel compositions in terrestrial mafic and ultramafic rocks. Journal of Petrology, 42, 2279-2302.

Bass, J.D., and Parise, J.B. (2008) Deep Earth and recent developments in Mineral Physics, Elements, 4, 157-163.

Born, M., and Huang, K. (1954) Dynamical theory of crystal lattices. Clarendon Press, Oxford. 420 p.

Bosi, F., Hålenius, U., and Skogby, H. (2010) Crystal chemistry of the $MgAl_2O_4$-$MgMn_2O_4$-$MnMn_2O_4$ system: Analysis of structural distortion in spinel and hausmannite-type structures. American Mineralogist, 95, 602-607.

Bosi, F., Hålenius, U., Andreozzi, G.B., Skogby, H., and Lucchesi, S. (2007) Structural refinement and crystal chemistry of Mn-doped spinel: A case for tetrahedrally coordinated Mn^{3+} in an oxygen-based structure. American Mineralogist, 92, 27-33.

Bosi, F., Andreozzi, G.B., Hålenius U., and Skogby, H. (2011) Zn-O tetrahedral bond length variations in normal spinel oxides. American Mineralogist, 96, 594-598.

Chang, Z.P., and Barsch, G. R. (1973) Pressure dependence of single-crystal elastic constants and anharmonic properties of spinel. Journal of Geophysical Research, 78, 2418-2433.

Clayton, J.D. (2010) A nonlinear thermomechanical model of spinel ceramics applied to aluminum oxynitride (AlON). Journal of Applied Mechanics, 78, 011013-1.

Cummins, H.Z., and Shoen, E. (1972) Linear scattering from thermal fluctuations. *In:* Laser Handbook. Arecchi, F.T. and Schultz-DuBois, E.O., North Holland Publishing Co. Amsterdam, pp 1029-1075.

Cynn, H., Anderson, O.L., and Nicol, M. (1993) Effects of cation disordering in a natural $MgAl_2O_4$ spinel observed by rectangular parallelepiped ultrasonic resonance and Raman measurements. Pure and Applied Geophysics, 141, 415-444.

Duffy, T.S., and Vaughan, M.T., (1988) Elasticity of Enstatite and its relationship to crystal structure. Journal of Geophysical Research, 93, 383-391.

Every A. G. (1980) General closed-form expressions for acoustic waves in elastically anisotropic solids. Physical Review B, 22, 1746-1760.

Fabian, D., Posch, T., Mutschke H., Kerschbaum, F., and Dorschner J. (2001) Infrared optical properties of spinels. Astronomy and Astrophysics, 373, 1125-1138.

Fierro, G., Lo Jacono, M., Dragone, R., Ferraris, G., Andreozzi, G.B., and Graziani, G. (2005) Fe-Zn manganite spinels and their carbonate precursors: preparation, characterization and catalytic activity. Applied Catalysis B: Environmental, 57, 153-165.

Finger, L.W., Hazen, R.M., and Hofmeister, A.M. (1986) High-Pressure crystal chemistry of spinel ($MgAl_2O_4$) and magnetite (Fe_3O_4): Comparisons with silicate spinels. Physics and Chemistry of Minerals, 13(4), 215-220.

Fregola, R.A., Bosi, F., and Skogby, H. (2011) A first report on anion vacancies in a defect $MgAl_2O_4$ natural spinel. Periodico di Mineralogia, 80, 28–37.

Frost, D.J. (2008) The upper mantle and transition zone. Elements, 4, 171-176.

Gelbmann, G., Krischanitz, R., and Jörg, S. (2013) Hybrid spinel technology provides performance advances for basic cement rotary kiln bricks. RHI Bulletin, 2, 10-12.

Giri, A.K., and Mitra, G.B. (1986) Elastic constants of solid solutions of ionic compounds. Journal of Physics D: Applied Physics 19, L5-L8.

Grimes, N.W. (1975) The spinels: versatile materials. Physics in Technology, 6, 22-27.

Hålenius, U., and Bosi, F. (2014) Color of Mn-bearing gahnite: A first example of electronic transitions in heterovalent exchange coupled $^{IV}Mn^{2+}$-$^{VI}Mn^{3+}$ pairs in minerals. American Mineralogist, 99, 261-266.

Hålenius, U., Bosi, F., and Skogby, H. (2007) Galaxite, $MnAl_2O_4$, a spectroscopic standard for tetrahedrally coordinated Mn^{2+} in oxygen-based mineral structures. American Mineralogist, 92, 1225-1231.

Hålenius, U., Bosi, F., and Skogby, H. (2011) A first record of strong structural relaxation of TO_4 tetrahedra in a spinel solid solution. American Mineralogist, 96, 617-622.

Hålenius, U., Skogby, H., and Andreozzi, G.B. (2002) Influence of cation distribution on the optical absorption spectra of Fe^{3+}-bearing spinel s.s.–hercynite crystals: evidence for electron transitions in $^{VI}Fe^{2+}$–$^{VI}Fe^{3+}$ clusters. Physics and Chemistry of Minerals, 29, 319-330.

Hålenius, U., Skogby, H., and Andreozzi, G.B. (2010) Structural relaxation around Cr^{3+} and the red-green color change in the spinel (sensu stricto)-magnesiochromite ($MgAl_2O_4$-$MgCr_2O_4$) and gahnite–zincochromite ($ZnAl_2O_4$–$ZnCr_2O_4$) solid solution series. American Mineralogist, 95, 456-462.

Hazen, R.M., and Jeanloz, R. (1984) Wustite ($Fe_{1-x}O$): A review of its defect structure and physical properties. Review of Geophysics and Space Physics, 22, 37-46.

Hazen, R. M. (1988) A useful fiction: polyhedral modeling of mineral properties. American Journal of Science, 288-A, 242-269.

Hazen, R.M. (1993) Comparative compressibilities of silicate spinels: anomalous behaviour of $(Mg,Fe)_2SiO_4$. Science, 259, 206-209.

Hazen, R.M. and Yang, H. (1999) Effects of cation substitution and order-disorder on P-V-T equations of state of cubic spinels. American Mineralogist, 84, 1956-1960.

Hill, R.J., Craig, J.R., and Gibbs, G.V. (1979) Systematics of the spinel structure type. Physics and Chemistry of Minerals, 4, 317-339.

Hong, J.O., and Yoo, H.I. (2006) Electric field-induced unmixing in mixed ferrite spinel $(Co,Fe)_3O_4$. Advances in Science and Technology, 46, 11-20.

Ito, M., Nagi, Y., Kado, N., Urukawa, S., Ogawa, T., Kondo, A., Koyama, K., Watanabe, K., and Kindo, K. (2011) Magnetic properties of spinel $FeCr_2S_4$ in high magnetic field. Journal of Magnetism and Magnetic Materials, 323, 3290-3293.

Jackson, I., Kanna, S.K., Revcolevschi, A., and Berthon J. (1990) Elasticity, shear-mode softening and high-pressure polymorphism of wüstite ($Fe_{1-x}O$). Journal of Geophysical Research, 95, 21671-21685.

Jacobsen, S.D., Reichmann, H.J., Spetzel, H.A., Mackwell, S.J., Smyth, J.R., Angel., R.J., and McCammon, C.A. (2002) Structure and elasticity of single-crystal (Mg,Fe)O and a new method of generating shear waves for gigahertz ultrasonic interferometry, Journal of Geophysical Research, 107, 2037.

Jörg, S., and Krischanitz, R. (2006) ANKRAL XE – First in service results of the new magnesia galaxite bricks. RHI Bulletin, 3, 7-10.

Juhin, A., Calas, G., Cabaret, D., Galoisy, L. and Hazemann, J.-L. (2007) Structural relaxation around substitutional Cr^{3+} in $MgAl_2O_4$. Physical Review B, 76, 054105.

Kiefer, B., Stixrude, L. and Wentzcovitch, R.M. (1997) Calculated elastic constants and anisotropy of Mg_2SiO_4 spinel at high pressure, Geophysical Research Letters, 24, 2841-2844.

Kocsis, V., Bordács, S., Varjas, D., Penc, K., Abouelsayed, A., Kuntscher, C.A., Ohgushi, K., Tokura, Y., and Kézsmárki, I. (2013) Magnetoelasticity in ACr_2O_4 spinels. Physical Review B, 87, 064416.

Levy, D., Diella, V., Pavese, A., Dapiaggi, M., and Sani, A. (2005) P-V equation of state, thermal expansion, and P-T stability of synthetic zincochromite ($ZnCr_2O_4$ spinel). American Mineralogist, 90, 1157–1162.

Levy, D., Pavese, A., and Hanfland, M. (2003) Synthetic $MgAl_2O_4$ (spinel) at high-pressure conditions (0.0001–30 GPa): A synchrotron X-ray powder diffraction study. American Mineralogist, 88, 93-98.

Levy, D., Pavese, A., Sani, A., and Pischedda, V. (2001) Structure and compressibility of synthetic $ZnAl_2O_4$ (gahnite) under high-pressure conditions from synchrotron X-ray powder diffraction. Physics and Chemistry of Minerals, 28, 612-618.

Levy, D., Pavese, A., and Hanfland, M. (2000) Phase transition of synthetic zinc ferrite spinel ($ZnFe_2O_4$) at high pressure, from synchrotron X-ray powder diffraction. Physics and Chemistry of Minerals, 27, 638-644.

Lewis, M.F. (1966) Elastic Constants of Magnesium Aluminate Spinel. Journal of Acoustic Society of America, 40, 728-729.

Li, Z., Fisher, E.S., Liu, J.Z., and Nevitt, M.V. (1991) Single-crystal elastic constants of Co-Al and Co-Fe spinels. Journal of Materials Science, 26, 2621-2624.

Lindsay, S. M., Anderson M. W., and Sandercock, J. R. (1981) Construction and alignment of a high performance multipass vernier tandem Fabry–Perot interferometer, Review of Scientific Instruments, 52, 1478–1486.

Liu, H.P., Schock, R.N., and Anderson, D.L. (1975) Temperature Dependence of Single-crystal spinel ($MgAl_2O_4$) elastic constants from 293 to 423 K measured by light-sound scattering in the Raman-Nath region. Geophys. J. R. Astr. Soc., 42, 217-250.

Lucchesi, S., Della Giusta, A., and Russo U. (1998) Cation distribution in natural Zn-aluminate spinels. Mineralogical Magazine, 62, 41-54.

Lucchesi, S., Russo, U., and Della Giusta, A. (1999) Cation distribution in natural Zn-spinels: franklinite. European Journal of Mineralogy, 11, 501–511.

Marquardt, H., Speziale, S., Jahn, S., Ganschow, S., and Schilling, F.R. (2009) Single-crystal elastic properties of $(Y,Yb)_3Al_5O_{12}$. Journal of Applied Physics, 106, 093519_1-5.

Nestola, F., Boffa Ballaran, T., Balic-Zunic T., Princivalle, F., Secco, L., and Del Negro A. (2002) Comparative compressibility and structural behavior of spinel $MgAl_2O_4$ at high pressures: the independency on the degree of cation order. American Mineralogist, 92, 1838-1843.

Nestola, F., Periotto, B., Andreozzi, G.B., Bruschini, E., and Bosi F. (2014) Pressure-volume equation of state for chromite and magnesiochromite: A single-crystal X-ray diffraction investigation. American Mineralogist, 99, 1248-1253.

O'Connell, R. J., and Graham, E.K. (1971) Equation of state of stoichiometric spinel to 10 Kbar and 800°C (abstract). EOS Transaction AGU 71, 359.

O'Neill, H.St.C. (1992) Temperature dependence of the cation distribution in zinc ferrite ($ZnFe_2O_4$) from powder XRD structural refinements. European Journal of Mineralogy, 4, 571-580.

O'Neill, H.St.C., and Dollase W.A., (1994) Crystal structures and cation distributions in simple spinels from powder XRD structural refinements: $MgCr_2O_4$, $ZnCr_2O_4$, Fe_3O_4 and the temperature dependence of the cation distribution in $ZnAl_2O_4$. Physics and Chemistry of Minerals, 20, 541-555.

O'Neill, H.St.C. (2003) The influence of next nearest neighbours on cation radii in spinels: the example of the Co_3O_4-$CoCr_2O_4$ solid solution. Mineralogical Magazine, 67, 547-554.

519 Pearson, D.G., Brenker, F.E., Nestola, F., McNeill J., Nasdala, L., Hutchison, M.T., Matveev, S.,
520 Mather, K., Silversmit, G., Schmitz, S., Vekemans, B., and Vincze, L. (2014) Hydrous
521 mantle transition zone indicated by ringwoodite included within diamond. Nature 507, 221-
522 224.

523 Reichmann, H.J., and Jacobsen, S.D. (2006) Sound velocities and elastic constants of $ZnAl_2O_4$
524 spinel and implications for spinel-elasticity systematics. American Mineralogist, 91, 7,
525 1049-1054.

526 Reichmann, H.J., Jacobsen, S.D., and Boffa Ballaran, T. (2013) Elasticity of franklinite and trends
527 for transition-metal oxide spinels. American Mineralogist, 98, 601-608.

528 Shannon, R.D. (1976) Revised effective ionic radii and systematic studies of interatomic distances
529 in halides and chalcogenides. Acta Crystallographica, A32, 751-767.

530 Sickafus, K.E., Wills, J.M., and Grimes N.W. (1999) Structure of spinel. Journal of the American
531 Ceramic Society, 82, 3279–3292.

532 Sinogeikin, S.V., and Bass, J.D. (2000) Single-crystal elasticity of pyrope and MgO to 20 GPa by
533 Brillouin scattering in the diamond cell. Physics of the Earth and Planetary Interiors, 120,
534 43-62.

535 Slagle, O.D., and McKinstry, H.A. (1967) Temperature dependence of the elastic constants of the
536 alkali halides. II. The solid solution KCl – KBr, Journal of Applied Physics, 38, 446 – 451.

537 Song, Q., and Zhang, J. (2004) Shape control and associated magnetic properties of spinel cobalt
538 ferrite nanocrystals. Journal of the American Chemical Society, 126, 6164–6168.

539 Speziale, S., Marquardt, H., and Duffy, T.S. (2014) Brillouin scattering and its application in
540 Geosciences. Reviews in Mineralogy & Geochemistry, 78, 543-603.

Speziale, S., Zha, C.S., Duffy, T.S., Hemley, R.J., and Mao, H.K. (2001) Quasi-hydrostatic compression of magnesium oxide to 52 GPa: Implications for the pressure-volume-temperature equation of state. Journal of Geophysical Research, 106, 512-528.

Suzuki, I., Ohno, I., and Anderson, O.L. (2000) Harmonic and anharmonic properties of spinel $MgAl_2O_4$. American Mineralogist, 85, 304-311.

Tomita, A., Sato, T., Tanaka, K., Kawabe, Y., Shirai, M., Tanaka, K., and Hanamura, E. (2004) Luminescence channels of manganese-doped spinel. Journal of Luminescence, 109, 19-24.

Urusov, V.S. (1992) A geometric model of deviation from Vegard's rule. Journal of Solid State Chemistry, 98, 223-236.

Velbel, M.A. (1999) Bond strength and the relative weathering rates of simple orthosilicates. American Journal of Science, 299, 679-696.

Waerenborgh, J.C., Figueiredo, M.O., Cabral, J.M.P., and Pereira, L.C.J. (1994) Temperature and composition dependence of the cation distribution in synthetic ZnFeyAl2-yO4 ($0 \leq y \leq 1$) spinels. Journal of Solid State Chemistry, 111, 300-309.

Webb, S.L., Jackson, I., and Fitz Gerald, J.D. (1988) High-pressure elasticity, shear-mode softening and polymorphism in MnO. Physics of the Earth and Planetary Interiors, 52, 117–131.

Whitfield, C.H. and Brody, E.M., and Basset, W.A. (1976) Elastic moduli of NaCl by Brillouin scattering at high pressure in a diamond anvil cell. Review of Scientific Instruments, 47, 942-947.

Yoneda, A. (1990) Pressure derivatives of elastic constants of single crystal MgO and $MgAl_2O_4$, Journal of Physics of the Earth, 38, 19-55.

Zener, C. (1947) Contributions to the theory of beta-phase alloys. Physical Review, 71, 846-851.

FIGURE CAPTIONS

FIGURE 1. Representative Brillouin spectrum for the sample Gx50. The peak for the quasi-longitudinal phonon is labeled as qL, qT1 and qT2 are the slow and the fast quasi-transverse phonons. The elastic peak (Rayleigh scattering) at the center of the spectrum is shaded while the signal from the diamonds windows is shown at the two far ends of the spectrum. Intensity is in arbitrary units.

FIGURE 2. Experimental data and calculated velocities for the sample Gx50 as a function of rotation angle (starting from an arbitrary position). Numbers between parentheses are the Miller indices of the plane on which the velocities were measured. Open diamonds are the quasi-longitudinal acoustic velocities (qL). Open triangles and circles represent the slow (qT1) and fast (qT2) quasi-transverse acoustic velocities, respectively. The symbol size is larger than experimental uncertainties. Solid curves are the velocities calculated using the best fit values of the elastic constants.

FIGURE 3. Elastic tensor components as a function of total Mn^{2+} mole fraction. The symbol size is sometimes larger than estimated uncertainties on the elastic constants. Solid lines are guides to the eye.

FIGURE 4. Aggregate bulk modulus (K_S) and shear modulus (G) as a function of total Mn^{2+} mole fraction. Where not shown the estimated uncertainties are smaller than the symbol size. Solid lines are guides to the eye.

FIGURE 5. Inversion degree as a function of Mn^{2+} mole fraction. The value for $MgAl_2O_4$ corresponds to disorder at 900 °C (Andreozzi et al. 2000). Estimated uncertainties (1σ) of the inversion degree are of the order of 0.05. Solid line is a guide to the eye.

585 **FIGURE 6.** Tetrahedral, octahedral and crystal bulk moduli as a function of total Mn^{2+} mole
586 fraction calculated according to Eq. 3 and using the fitted values of the $K_i^j s$ of Table 3. Solid lines
587 are guides to the eye.

588 **FIGURE 7.** Polyhedral bulk moduli as a function of the inversion degree (*i*). The sample
589 with the lowest value of *i* is the galaxite end-member (Gx100) while the sample with the greatest *i*
590 corresponds to Gx70. Dotted lines are linear regression of the data.

591 **FIGURE 8.** Specific polyhedral bulk moduli (K_i^j) of Mg, Mn^{2+} and Al in tetrahedral and
592 octahedral coordination plotted against ionic potential (expressed as valence units over ångström).
593 The ionic potentials were calculated starting from the values of the ionic radii given by Shannon
594 (1976). Dotted line is the linear (unweighted) regression of the data whose equation (Eq. 4) is
595 shown in the upper left of the graph.

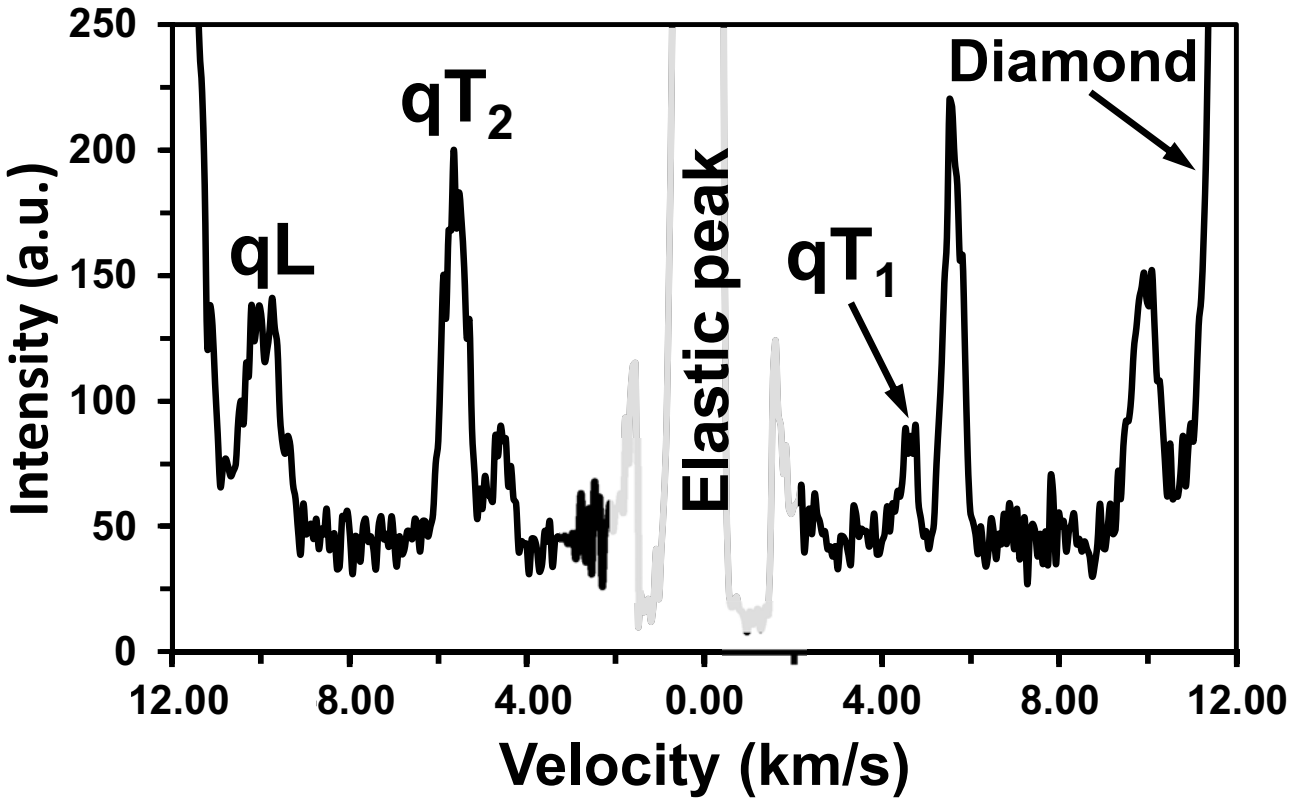
250
200
150
100
50
0
Intensity (a.u.)
qL
qT2
Elastic peak
qT1
Diamond
12.00
8.00
4.00
0.00
4.00
8.00
12.00
Velocity (km/s)

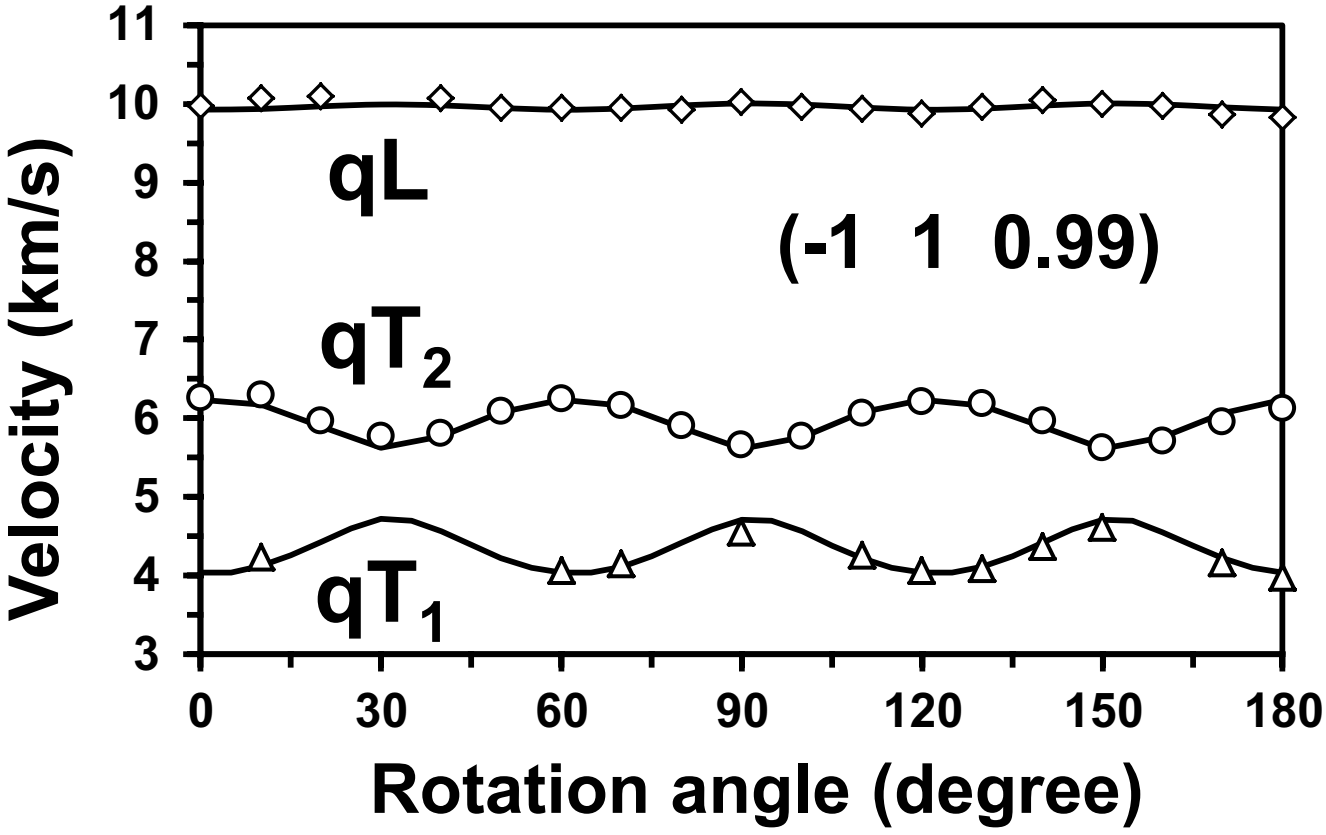
Velocity (km/s)
11
10
9
8
7
6
5
4
3
qL
(-1 1 0.99)
qT2
qT1
0
30
60
90
120
150
180
Rotation angle (degree)

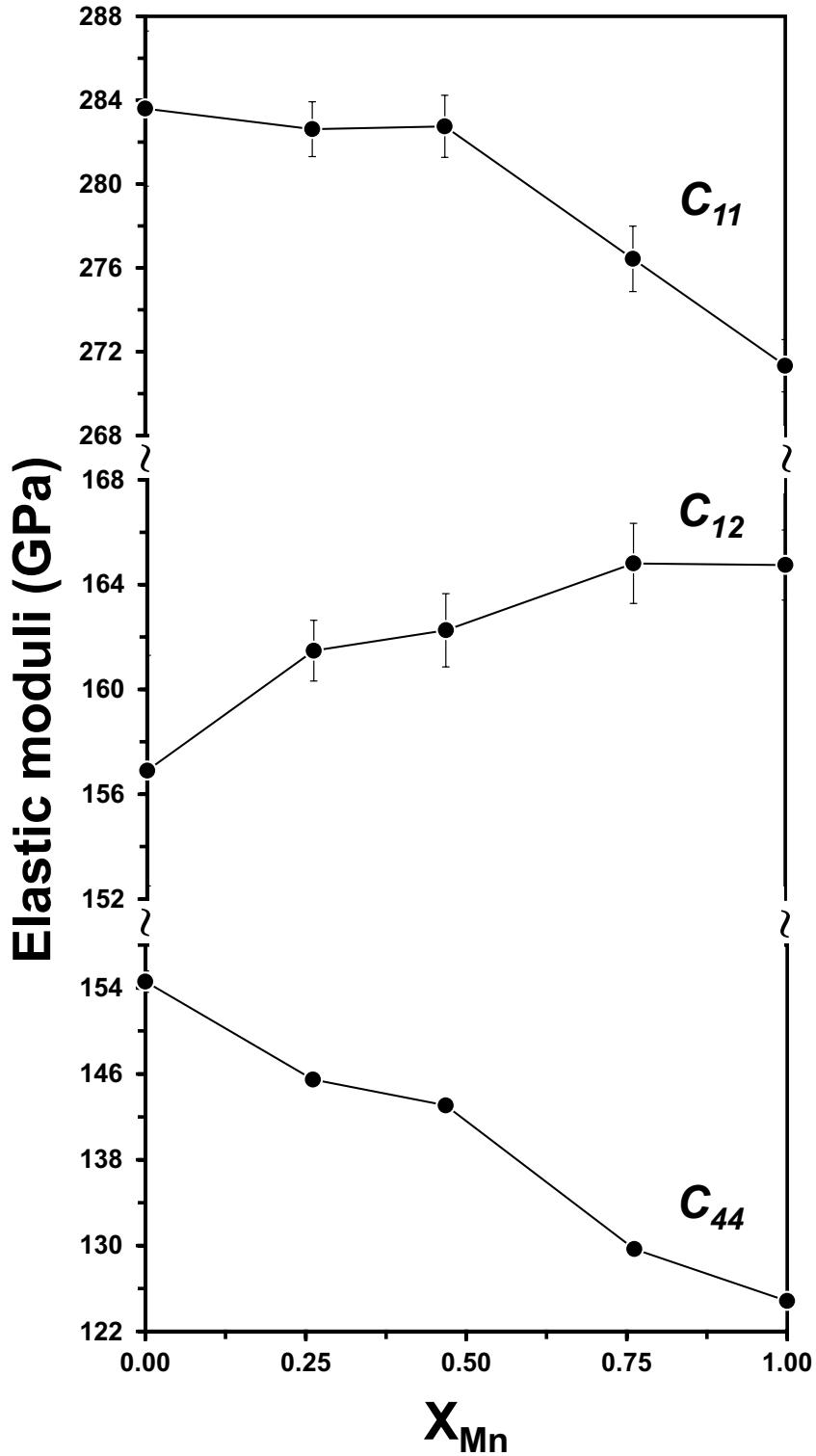
Elastic moduli (GPa)
288
284
280
276
272
268
168
164
160
156
152
154
146
138
130
122
C_{11}
C_{12}
C_{44}
0.00
0.25
0.50
0.75
1.00
X_{Mn}

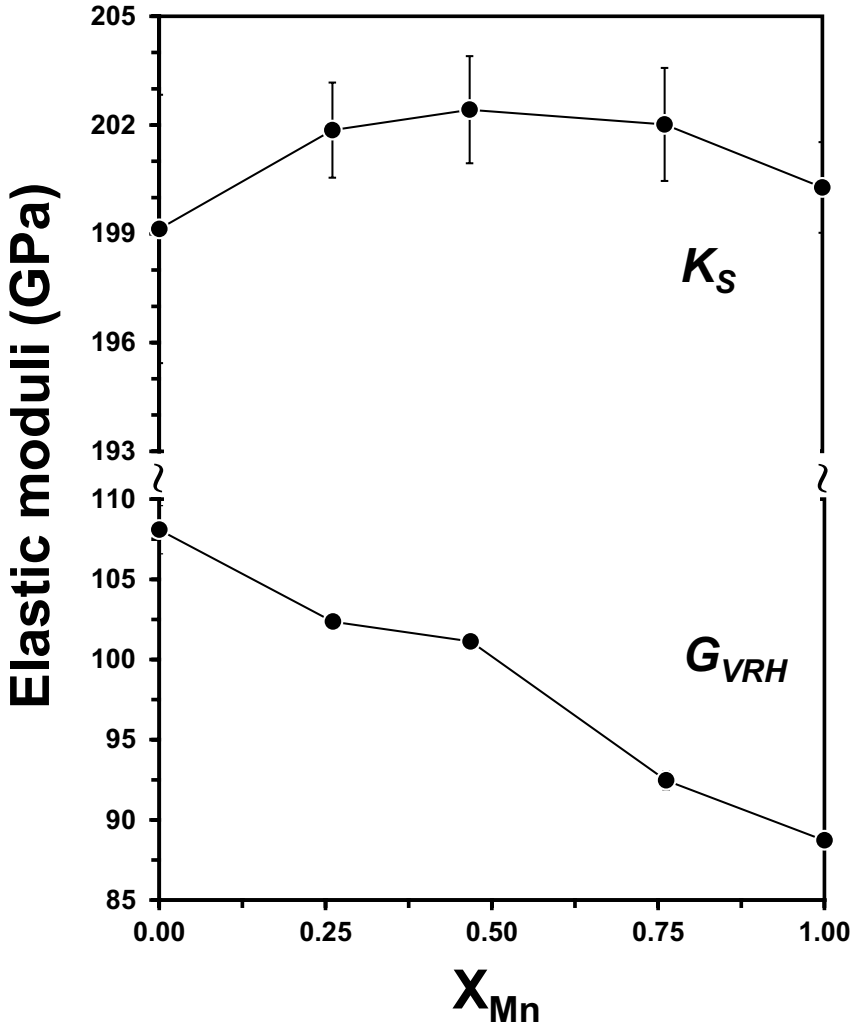
Elastic moduli (GPa)
205
202
199
196
193
110
105
100
95
90
85
K_S
G_{VRH}
0.00
0.25
0.50
0.75
1.00
X_{Mn}

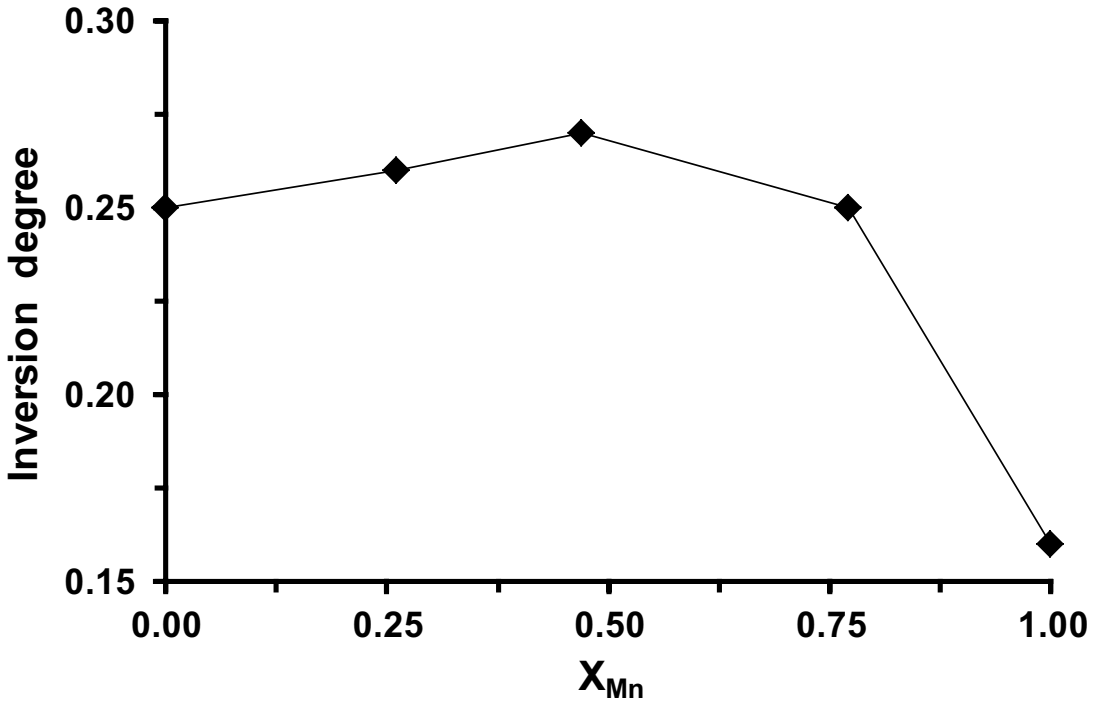
0.30
0.25
0.20
0.15
Inversion degree
0.00
0.25
0.50
0.75
1.00
X_{Mn}

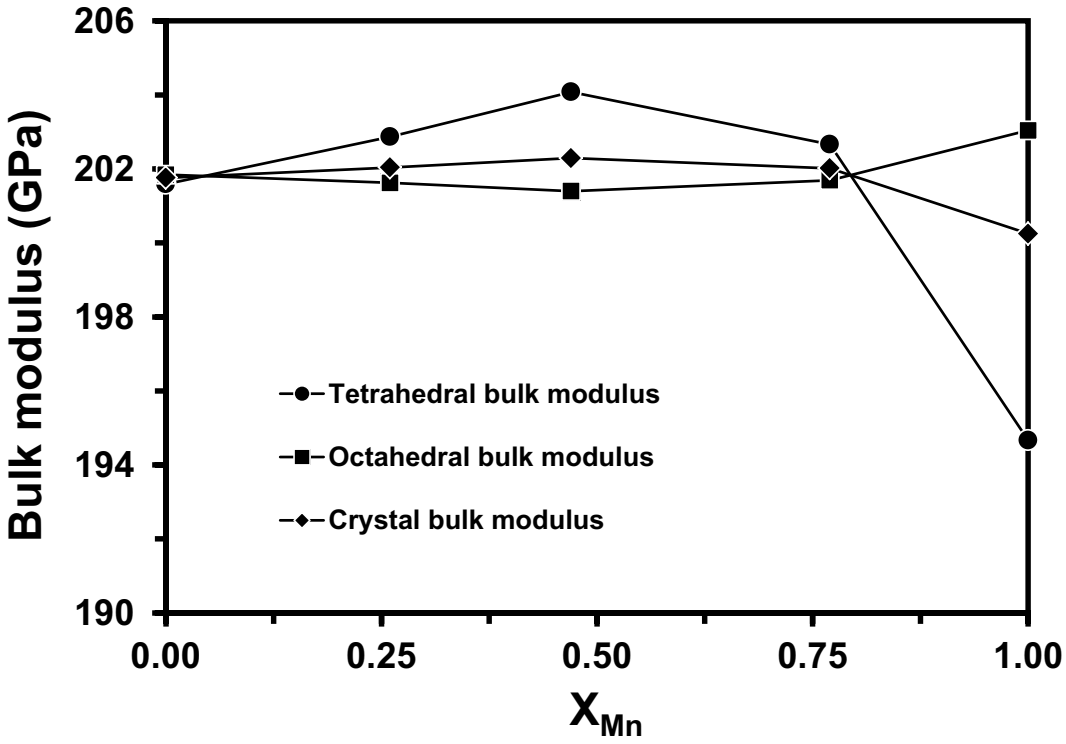
206
202
198
194
190
Bulk modulus (GPa)
0.00
0.25
0.50
0.75
1.00
X_{Mn}
Tetrahedral bulk modulus
Octahedral bulk modulus
Crystal bulk modulus

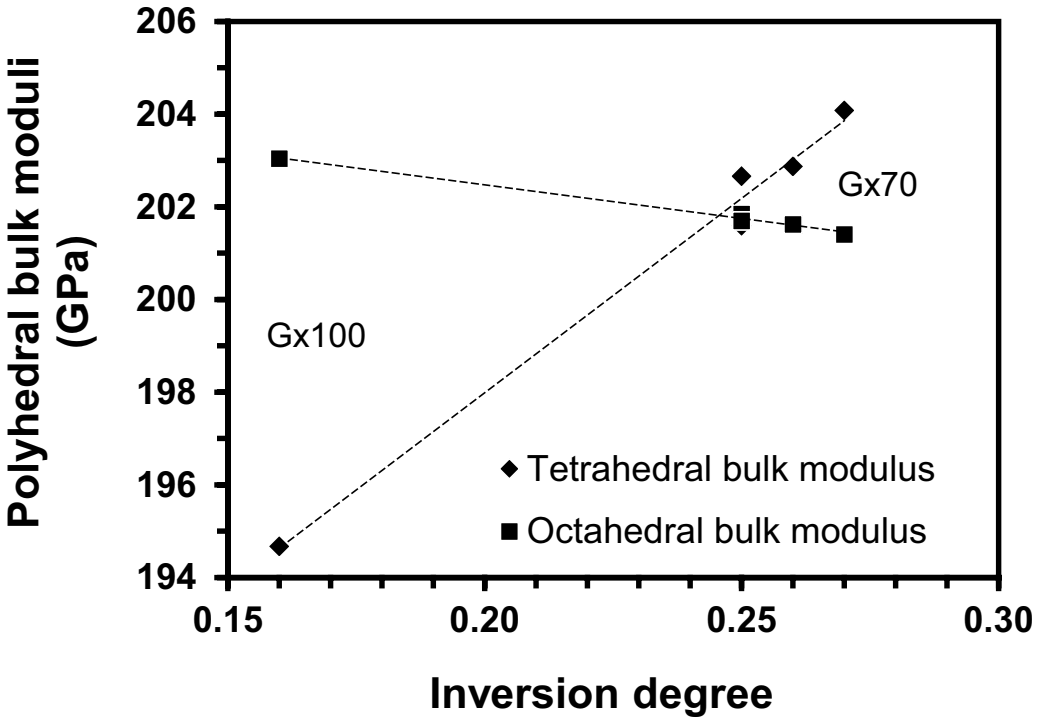
Polyhedral bulk moduli (GPa)
206
204
202
200
198
196
194
0.15
0.20
0.25
0.30
Inversion degree
Gx70
Gx100
Tetrahedral bulk modulus
Octahedral bulk modulus

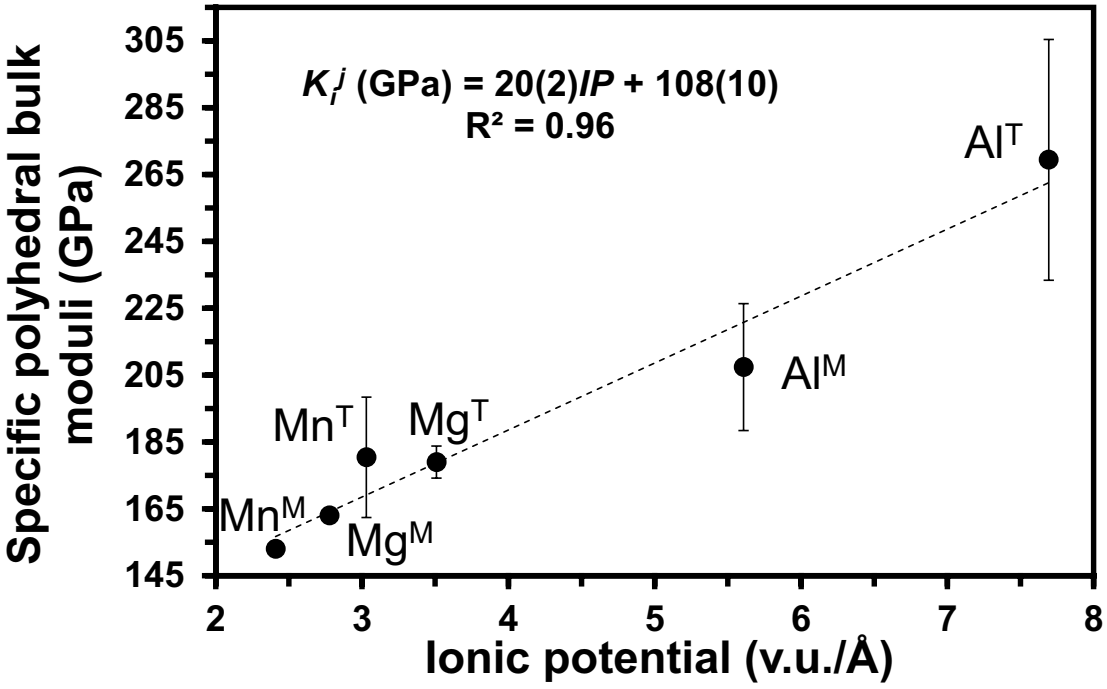
K_i^j (GPa) = 20(2)*IP* + 108(10)
R² = 0.96
Specific polyhedral bulk moduli (GPa)
Ionic potential (v.u./Å)
305
285
265
245
225
205
185
165
145
2
3
4
5
6
7
8
Al^T
Al^M
Mn^T
Mg^T
Mn^M
Mg^M

Table 1.Mole fraction of Mn, density and elastic parameters for the $MgAl_2O_4$-$MnAl_2O_4$ series.

Sample	X_{Mn}	Density (g/cm^3)	C_{11} (GPa)	C_{12} (GPa)	C_{44} (GPa)	K_S (GPa)	G_{VRH} (GPa)	C_{11}-C_{12} (GPa)	E (GPa)	ν
$MgAl_2O_4$*	0.000	3.57	283.6(3.7)	156.9(4.4)	154.6(1.0)	199.1(4.1)	108.1(1.5)	02.3(4.5)	274.6(4.4)	0.270(0.010)
Gx 50	0.261	3.73	282.6(1.3)	161.5(1.2)	145.5(0.5)	201.9(9)	102.4(5)	16.0(1.3)	262.8(1.4)	0.283(0.002)
Gx70	0.468	3.86	282.7(1.5)	162.3(1.4)	143.1(0.5)	202.4(1.1)	101.1(6)	19.2(1.5)	260.0(1.7)	0.286(0.003)
Gx 90	0.762	4.02	276.4(1.6)	164.8(1.5)	129.7(0.6)	202.0(1.1)	92.5(6)	35.1(1.6)	240.8(1.7)	0.301(0.003)
Gx 100	1.000	4.15	271.3(1.3)	164.8(1.3)	124.9(0.5)	200.3(1.0)	88.7(5)	39.9(1.4)	231.9(1.4)	0.307(0.003)

Notes: X_{Mn} values are from Hålenius et al. (2007; 2011). Density calculated from the empirical formula. C_{11}, C_{12}, C_{44} are the components of the single crystal elastic tensor. K_S and G_{VRH} are the average isentropic bulk modulus and shear modulus respectively. E is the average Young modulus and ν is the average Poisson's ratio. *Elastic parameters as the average values (with 1σ standard deviation in parenthesis) of the extant literature data (Lewis 1966; Chang and Barsch 1973; Liu et al. 1975; Yoneda 1990; Askarpour et al. 1991; Cynn et al. 1993). Numbers in parentheses are estimated uncertainty (1σ).

Table 2. Cation site population of studied Mn-spinels (data from Hålenius et al. 2007; 2011)

Sample	Gx50	Gx70	Gx90	Gx100
		T-site		
Mg (apfu)	0.48	0.26	0.01	0.00
Mn^{2+}	0.26	0.47	0.74	0.84
Al	0.26	0.27	0.25	0.16
sum	1.00	1.00	1.00	1.00
		M-site		
Mg	0.26	0.27	0.22	0.00
Mn^{2+}	0.00	0.00	0.03	0.16
Al	1.74	1.73	1.75	1.84
sum	2.00	2.00	2.00	2.00

Table 3. Ionic potentials (*IP*) and fitted values of the specific polyhedral bulk moduli (K_i^j) for Mg, Mn^{2+} and Al at T and M.

Cation	*IP* (vu/Å)	K_i^T (GPa)	*IP* (vu/Å)	K_i^M (GPa)
	T-site		M-site	
Mg	3.51	179(5)	2.78	163(0.9)*
Mn^{2+}	3.03	180(18)	2.41	153(2.0)*
Al	7.70	270(36)	5.61	207(19)

Note: *Not refined values. Numbers in parentheses are estimated uncertainty. The uncertainties were estimated using the jackknife resampling technique.